Chromium Adsorption Reveals a Persistent Hydroxylation of Vacuum-Annealed α-Al 2 O 3 (0001)

Maya Messaykeh, Jacek Goniakowski, Gregory Cabailh, Jacques Jupille, Rémi Lazzari, Pierre Lagarde, Nicolas Trcera

Chromium Adsorption Reveals a Persistent Hydroxylation of Vacuum-annealed α-Al_2O_3(0001)

Maya Messaykeh,[1] Jacek Goniakowski, [1*] Gregory Cabailh, [1*] Jacques Jupille, [1] Rémi Lazzari, [1] Pierre Lagarde, [2] and Nicolas Trcera[2]

[1] *Sorbonne Université, CNRS-UMR 7588, Institut des Nanosciences de Paris, F-75252 Paris Cedex 05, France*
[2]*Synchrotron SOLEIL, L'Orme des Merisiers, Saint-Aubin, BP 48, F-91192 Gif sur Yvette, France*

**corresponding authors*
Gregory Cabailh : gregory.cabailh@sorbonne-universite.fr
Jacek Goniakowski : jacek.goniakowski@insp.jussieu.fr

Abstract

We address herein the question of the termination of the Al-terminated α-Al_2O_3(0001) surface. Over decades, various analyses made by different groups repeatedly suggested the presence of a residual coverage of surface OH groups on Al_2O_3 crystals and powders after annealing in vacuum. However, other authors came to contrary conclusions, thus maintaining a persistent blur on the issue. The present work examines the Cr/alumina interface via Cr K absorption edge analysis (Extended X-Ray Absorption Fine Structure and X-ray Absorption Near Edge Structure) and photoemission with the support of density functional (DFT) calculations. Experiments support the presence of surface OH groups to account for the observed environment as well as the oxidation state of Cr adatoms (Cr^{3+}). Following a comprehensive DFT-based analysis of Cr^{z+}-O_nH_m configurations (z=0 to 6, n and m=0 to 3), the Cr^{3+}-O_2H alumina-supported surface moieties are found to successfully fit the XAS edge calculations. Most importantly, the combination of experiment and theory that is developed unambiguously demonstrates the presence of surface OH groups on α-Al_2O_3(0001) after annealing in vacuum.

1. Introduction

A wealth of experiments and calculations have been devoted to the α-Al_2O_3(0001) surface which currently serves as a model for alumina surfaces to overcome the complexity of real cases in geochemistry[1,2], catalysis[3], electronics[4] and ceramic industry[5]. The α-Al_2O_3 phase won the favor of experimentalists for its thermodynamic stability at standard temperature and pressure conditions[6] and also for the prosaic reason that it is the only alumina polymorph commercially available in the form of centimeter-sized crystals. An additional motivation came from the ease with which the α-Al_2O_3(0001) surface hydroxylates by dissociative adsorption of water. Unlike some other common oxides such as MgO whose hydroxylation is still the subject of debate[7,8], there was an early consensus between photoemission[9,10], high-resolution electron energy loss spectroscopy[9,11-13], thermal desorption[14], *ab initio* molecular dynamics[15] and density functional approaches[16,17], that α-Al_2O_3(0001) adsorbs dissociatively isolated water molecules. This is because the out-of-plane 2p orbitals of the coordinatively unsaturated aluminum ions that terminate the α-Al_2O_3(0001) surface give those sites a strong acidic Lewis character[15-17].

Surface hydroxyl groups considerably modify the behavior of the oxide. They affect metal-alumina interfaces with consequences that can however go in opposite directions for species of different nature.

Depending on their density or on their interaction with the adsorbate under consideration[18], surface OH groups may favor the nucleation and increase the density of supported clusters[19,20], strengthen the cluster adhesion[21,22] or, conversely, weaken their binding[22,23]. On hydroxylated α-Al_2O_3, Al[24,25], Zn[26,27] and transition metals such as Rh[19,20], Ti[24,25], Co[4] and Cu[28,29] oxidize according to the activated reaction of the following type:

$$nOH^- + Me^0 \rightarrow nO^{2-} + Me^{n+} + nH$$

Hydroxyl groups were often assumed to intervene in the not yet understood termination of the oxide. The α-Al_2O_3(0001) surface undergoes a series of complex Al-rich reconstructions at high temperatures under Ultra-High Vacuum (UHV) up to the (√31x√31)R±9° structure[30-33]. Reconstructions are associated to the disappearance of O in the last atomic planes of the corundum structure. Ion scattering[34] revealed that, after annealing up to temperatures as high as 1373 K under UHV but below the onset of reconstructions, the (1x1)-terminated alumina surface retains a residual coverage of hydrogen that was tentatively attributed to surface OH groups. These observations are not limited to single crystals analyzed under ultra-high vacuum since, in a much more general way, a residual coverage of 2.6 $OH.nm^{-2}$ on nanocrystalline α-Al_2O_3 was shown to resist outgassing conditions[6]. An O 1s chemical shift toward higher binding energy obtained after a similar treatment was later assigned to residual OH groups[24,25,28,29] although a different interpretation attributed the shift to surface oxygen atoms[35]. In addition, the ability of the α-Al_2O_3(0001) surface to dissociate the isolated water molecule was questioned by two series of experiments. After an Ar ion sputtering followed by annealing at 1040 K[36,37], a crystal removed from the ultra-high vacuum chamber could be exposed to air for days without significant hydroxylation, as analyzed by vibrationally resonant sum frequency generation[37]. A similar inertness was observed after cleaning the alumina surface by neon ion sputtering[38]. However, surface OH coverage of α-Al_2O_3(0001) surface has also been shown to resist Ar ion sputtering[28,29], highlighting the importance of preparation conditions. As far as our goal is to deal with hydroxylated surfaces, our preparation is thus similar to that in references [24,25,28,29,33].

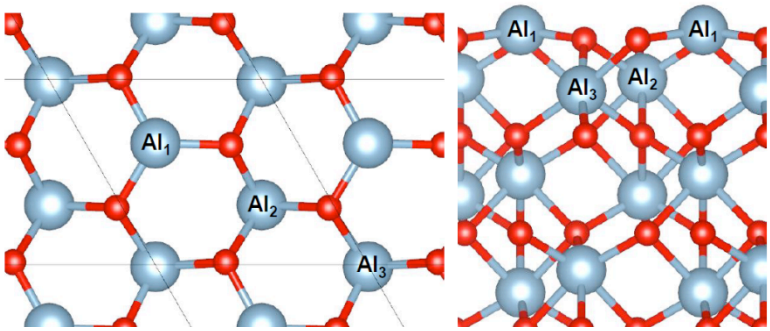

Fig. 1 Representation of the α-Al_2O_3(0001) surface: left, top view of the surface layer; right, side view of the surface; the surface Al, intermediate Al, deep Al, are labelled Al_1, Al_2, and Al_3, respectively. Oxygen and aluminum atoms are represented by large red and small light blue spheres.

The present work was inspired by the transition metal buffer layers that are widely used to enhance the adhesion at poorly wetting metal-oxide interfaces, alumina being often encountered in this respect[21,25,35,39-41]. The understanding of how buffers work requires the knowledge of the interface structure and chemistry at the atomic level. We focus herein on Cr buffer layers that were predicted by density functional theory (DFT) calculations to be quite efficient to promote the Zn adhesion on alumina under realistic conditions which is an issue in the galvanization process of the so-called high

strength steels (AHSS) grades. These grades were developed to manufacture thinner steel sheets and reduce the weight of the automotive vehicles to meet the environmental imperative of CO_2 emission reduction. They involve electro-positive strengthening elements, including Al[21,26,42,43], whose oxygen-induced segregation during the steel sheet fabrication leads to the formation of surface oxide layers that prevent the adhesion of the anti-corrosive Zn protection during the galvanization process. The present work only deals with the Cr/alumina interface. The Zn/Cr/alumina stacking will be examined in a forthcoming paper. The α-Al_2O_3(0001) surface retained herein is the surface annealed at high temperature under ultra-high vacuum which corresponds, if not to the Al-terminated bare substrate, at least to the termination involving the lowest hydroxyl coverage. The Cr/alumina film is studied by a combination of X-ray absorption spectroscopy (Extended X-ray Absorption Fine Structure (EXAFS) and X-ray Absorption Near Edge Structure (XANES)), laboratory X-ray photoemission (XPS) and numerical simulations relying on DFT. The EXAFS technique proved efficient in studying submonolayer coverage of adatoms[44-47]. The possible presence of non-periodically arranged[34] residual OH groups maintains a persistent blur on the nature of the non-polar Al-terminated α-Al_2O_3 (0001) surface (Fig. 1). The objective is both to determine the site and chemistry of chromium atoms at the α-Al_2O_3(0001) surface and to examine whether there are interactions of metal adatoms with surface hydroxyl groups.

	Cr thickness (Å)			Cr local order – Results of fits	
	Average value	Quartz balance data	K edge data	Cr-O (N ± 0.3, R ± 0.02 Å)	Cr-Cr (N ± 0.5, R ± 0.05 Å)
Cr/ α-Al_2O_3(0001)	**0.24**	0.3	0.18	3.7 O @ 1.95 Å	
	1.05	1	1.1	3.7 O @ 1.93 Å	1 Cr @ 2.86 Å
	1.5	1.5	1.5	3.1 O @ 1.92 Å	1 Cr @ 2.94 Å
	2.35	2.5	2.2	2.3 O @ 1.92 Å	4 Cr @2.85 Å
	15*	15*	15*	1.5 O @1.95 Å	1 Cr @ 2.5 Å 2 Cr @ 2.92 Å
Cr_2O_3				6 O @ 1.94 Å	4 Cr @ 2.96 Å (2-shell fit)
Cr metal					8 Cr @ 2.52 Å 6 Cr @ 2.91 Å

*value determined by the quartz balance and used to calibrate the Cr K edge jump.

Table 1. Modeling of the EXAFS spectra recorded at the Cr K edge on the different Cr/α-Al_2O_3(0001) films studied herein. The O and Cr shell around the Cr adatoms are defined by a distance R and a number N of atoms. Analysis of the oxide Cr_2O_3 and of the pure metal are given for comparison. As a reference, Cr thickness of 1Å (quartz balance) corresponds to about 0.09 Cr atom/A^2.

2. Experimental and computational

Experiments have been performed on the LUCIA beamline at synchrotron SOLEIL (St Aubin, France) in an UHV apparatus which involves a preparation and a main chamber already described[46,47]. The surfaces of the α-Al_2O_3(0001) single crystals were annealed in the first chamber at ~1500 K in front of a gas doser under a stationary oxygen partial pressure of ~ $1x10^{-6}$ mbar. The cleanliness of the surface was controlled by Auger spectroscopy and Low-Energy Electron Diffraction (LEED) revealed a (1x1)-

termination. Then Cr was deposited in the preparation chamber from an electron-bombarded pure Cr rod that was carefully outgassed (EFM3-Omicron evaporator). The Cr flux was calibrated by a quartz balance set at the sample position. Deposition rates were typically of the order of 1 Å in 15 minutes. Each coverage explored corresponded to a new clean sample. Once transferred in the main chamber, the Cr-covered crystals were analyzed by XAS. XANES and EXAFS spectra were collected at the Cr K-edge (around 6000 eV) by using a Si(111) monochromator in Total Electron Yield (TEY). XAS spectra for pure Cr metal and Cr_2O_3 oxide were collected as reference compounds. Although samples were found carbon free after preparation, a segregation of Ca up to a 0.1 ML coverage was detected by Auger spectroscopy on some samples after annealing at high temperature. Most importantly, the presence of surface Ca does not induce any change in the Cr edges. Attempts to involve Ca, a heavier element than Al and O, in the environment of Cr in the EXAFS data modeling were unsuccessful. Therefore, from a spectroscopic point of view, Ca is absent from the chemical surrounding of Cr. Additional X-ray Photoemission Spectroscopy (XPS) analysis was performed at the INSP (Paris, France) on various Cr/α-Al_2O_3(0001) thicknesses by using a non-monochromatic Mg-Kα excitation with a hemispherical analyzer (Phoibos from SPECS company).

Calculations regarding Cr adsorption on the α-Al_2O_3(0001) surface were performed within the framework of the DFT approach with the Vienna Ab-initio Simulation Package (VASP)[48,49] using the Projector Augmented Wave (PAW) method[50,51] to represent the electron-core interaction and a 400 eV energy cutoff in the development of spin-polarized Kohn-Sham orbitals on a plane-wave basis set. Dispersion-corrected (optB88-vdW)[52-54] exchange-correlation functional was employed. Ionic charges were estimated with the partition scheme proposed by Bader[55,56] and magnetic moments were obtained by integration of the spin density within the Bader volumes. Atomic configurations were plotted with VESTA[57].

We have considered the Al-terminated Al_2O_3 (0001) surface with a single Cr adatom/substitution and with alternative O_nH_m (n, m = 0-3) hydroxylation layers per (1×1) surface cell. The alumina substrate was represented by a slab composed of six Al_2O_3 layers with an experimental in-plane bulk lattice parameter of 4.785 Å. The hydroxylation layer and Cr adatoms were adsorbed on one side of the alumina slab only and the coordinates of all atoms were allowed to fully relax until forces got lower than 0.01 eV $Å^{-1}$. The Brillouin zone of the (1×1) cell was sampled with a Γ-centered (8 × 8 × 1) Monkhorst-Pack mesh. The relative thermodynamic stabilities of the considered surface Cr+O_nH_m configurations were estimated from their formation energies:

$$\Delta E = E(Cr+O_nH_m/Al_2O_3) - E(Al_2O_3) - E(Cr) - n[\Delta\mu_O + 1/2E(O_2)] - m[\Delta\mu_H + 1/2E(H_2)]$$

where $E(Cr+O_nH_m/Al_2O_3)$ and $E(Al_2O_3)$ are the total energies of adsorbate-covered and bare alumina slabs, respectively, and E(Cr) is the total energy of an isolated Cr atom. The oxygen and hydrogen chemical potentials μ_X are referred to the total energies $E(O_2)$ and $E(H_2)$ of the diatomic O_2 and H_2 molecules, respectively with $\mu_X = \Delta\mu_X + E(X_2)$. With this choice $\Delta\mu_X = 0$ represents X-rich conditions (molecular condensation) and the physically relevant potentials correspond to $\Delta\mu_X < 0$.

Theoretical XANES spectra were calculated by using the FDMNES software[58]. This method is based on the finite-difference algorithm (FDM), where the shape of the potential is calculated self-consistently. This avoids the use of the muffin-tin approximation which hardly represents the interatomic potential in ionic solids. The energy dependent exchange-correlation potential is obtained following the Hedin and Lundqvist approach[59]. XANES spectra were obtained with an energy broadening using an arctangent formula. The XANES calculations were performed with energy steps of 1 eV in the pre-edge region, 0.1 eV in the XANES region and finally 1 eV for the end up to 120 eV

after the XANES region. The structures used in the input files were taken from the calculations performed by VASP allowing the best fit results for the EXAFS analysis.

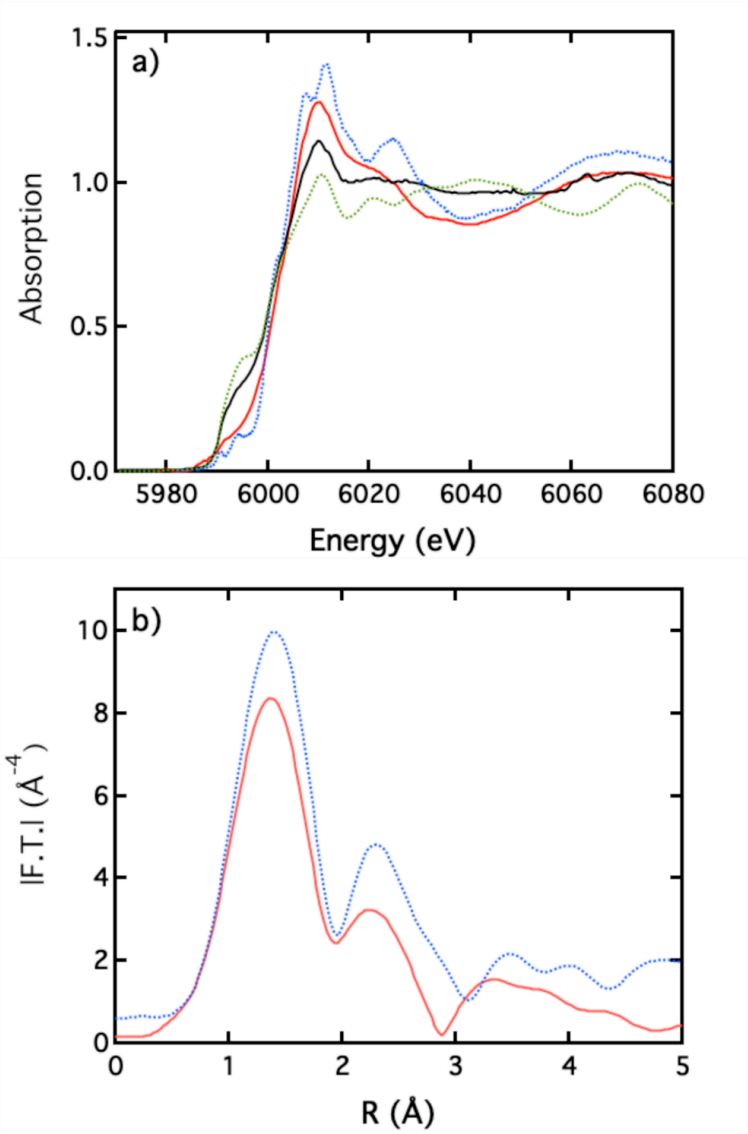

Fig. 2 – XAS spectra at the Cr K absorption edge: (a) XANES spectra of Cr_2O_3 (blue), Cr metal (green), 1.05 Å and 15 Å Cr/α-Al_2O_3(0001) film (red and black, respectively); (b) Modulus of the Fourier Transforms of the EXAFS collected on the 1.05 Å Cr/α-Al_2O_3(0001) film (red), and on a bulk Cr_2O_3 sample (blue).

1. Experimental results

Five Cr/α-Al_2O_3(0001) deposits were analyzed by EXAFS. The thickest film (15 Å, as determined by the quartz balance) was used to calibrate the Cr K edge jump. The good agreement between the values of the film thickness directly determined by the quartz balance and those derived from the relative edge jump, prompted us to retain the average values which range from 0.24 to 15 Å (Table 1). Incidentally, this points at a Cr/Al_2O_3 sticking coefficient close to one. Fig. 2a compares the Cr K near edge structure (XANES) recorded on the 1.05 Å thick Cr/alumina film to spectra from metallic chromium and pure Cr_2O_3 oxide. The energy edge position and the overall shape of the near edge

spectrum show a strong similarity with Cr^{3+} in the Cr_2O_3 oxide and definitely discard Cr^{2+} and Cr^{6+} states. However, the presence of Cr^{4+} in CrO_2, which is expected at slightly higher energy, cannot be rejected. The point will be discussed on the basis of the DFT calculations. For the thicker deposits a contribution at lower energy assigned to Cr metal is clearly visible (Fig. 2b).

The extraction and analysis of the EXAFS data from the Cr K edge x-ray absorption spectra was done with the Athena and Artemis software[60]. Fourier Transforms (FT), with a Kaiser-Bessel apodisation window, were limited to 8.5 $Å^{-1}$ due to diffraction peaks coming from the substrate. The quantitative analysis makes use of phase functions coming from a FEFF9 calculation[61] checked on Cr metal and Cr oxide. In Cr_2O_3, Cr atoms are surrounded by three oxygen atoms at 1.92 Å and three oxygen atoms in next-near-neighbor positions at 2.07 Å. Neighboring Cr atoms are found at 2.9 Å and 3.3 Å. Actually, as a first approach to a quantitative analysis and because of the rather short energy domain of the EXAFS spectra which limits the distance resolution, a good modeling of Cr_2O_3 can be obtained by considering only an average oxygen shell at 1.94 Å and a Cr shell at 2.96 Å (Table 1). In a similar way, in order to reduce the number of free parameters in the description of the Cr deposits, the EXAFS analysis was performed for all the samples by considering that Cr atoms are only surrounded by an oxygen shell and a chromium shell. The similarity of the Cr-O distance of 1.92-1.95 Å found for all Cr/alumina samples (Table 1) with the Cr-O distance found in Cr_2O_3, is a first proof of the formation of Cr^{3+} in an environment close to that of the oxide. Actually, the near-edge spectrum of the deposit (Fig. 2a) appears as a smoothed version of the Cr_2O_3 one, which means a similar environment of Cr, but with some disorder with respect to the pure crystalline oxide. On the thicker films, (Fig. 2b) the presence in the near-edge spectrum of a signature characteristic of Cr metal (around 5995 eV) and the general shape in the range 6000-6030 eV show that chromium metal clusters are also formed on the surface. Based on the two-shell approach, the chemical environment evolves with the film thickness. As it increases, we observe a progressive apparition of Cr-Cr mean distances ranging between those found in the oxide (2.96 Å) and in the metal (2.52 Å). As a consequence, the apparent coordination number with oxygen decreases because of the renormalisation by the total number of Cr atoms. Quite importantly, the finding of more than three atoms in the O shell surrounding the Cr atoms (Table 1) reveals the presence of extra oxygen atoms with respect to the three surface atoms that are expected from a Cr adsorption on a bare Al-terminated α-Al_2O_3(0001) surface (Fig. 1). This is illustrated in Fig. 2c by the comparison of the modulus of the EXAFS Fourier Transform of pure Cr_2O_3 to that of the same 1.05 Å thick Cr/α-Al_2O_3(0001) film as in Fig. 2a. A more detailed analysis is presented below for the thinner deposit for which a precise structural model can be really built.

Photoemission (XPS) measurements were performed on the Al 2s and O 1s core level spectra of α-Al_2O_3(0001) after Cr deposition to determine the origin of the Cr oxidation (Fig. 3). The 0.8 Å thick Cr film is close to the one analyzed in details by EXAFS (Fig. 2) which exhibits Cr-O and Cr-Cr distances similar to those found in the oxide (see below). Deposition does not induce any change in the Al 2s profile although a shift of -2.8 eV is expected for metallic Al relative to alumina[25]. Thus, reduction of alumina at the Cr/α-Al_2O_3(0001) interface is discarded[62]. Nevertheless, in parallel, a component is removed on the higher binding energy side of the O1s spectrum, while another component appears on the lower binding energy side (Fig. 3b). Those observations suggest that the formation of chromium ions does not stem from a reduction of alumina but from a reaction of Cr adatoms with surface hydroxyl groups. Similarly, XPS analysis of the Ti/α-Al_2O_3(0001) interface[24,25] suggested the formation of Ti^{4+} ions via a reaction of Ti with surface hydroxyl groups. However, the determination of the oxidation state which was possible for Ti/alumina[24,25] is prevented herein by the complexity of the Cr core level. Photoemission spectra indicate clearly that Cr is oxidized, but the degree of oxidation is out of grasp because of charge effects. Finally, one may wonder whether the residual pressure, in particular water vapor, is involved in the observed oxidation of Cr. During

experiments, the recording of the Cr K edge spectrum began ca.10 minutes after Cr deposition, which corresponds to the time needed for the transfer of the sample from the preparation to the main chamber. Then, successive EXAFS spectra were collected each 10 to 20 minutes. Therefore, the short time between Cr deposition and the recording of the first Cr K edge spectrum did not allow a significant oxidation of the deposited Cr by the residual pressure. The main proof of the weakness of the contribution of the residual gases to the oxidation of Cr is that neither the near-edge – characteristic of Cr^{3+}- Cr^{4+} oxidation state – nor the EXAFS of the successive spectra were perceptibly modified with time, even in the case of the observation of a metallic Cr^{0} component.

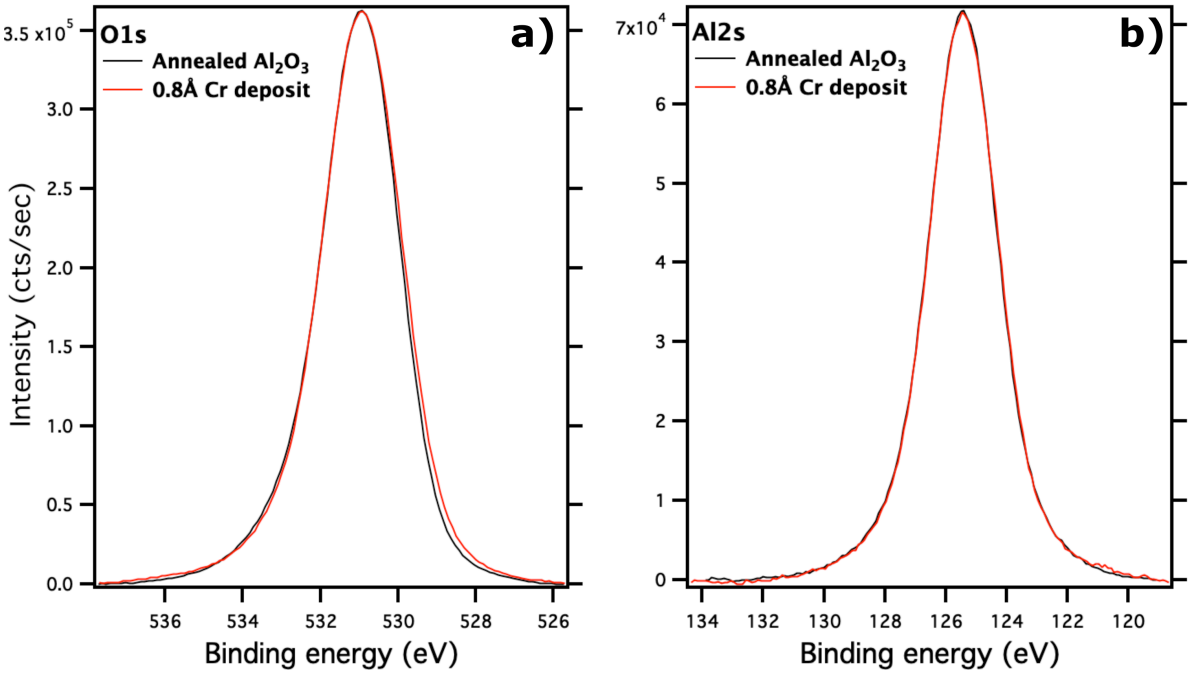

Fig. 3 – Evolution of photoemission spectra upon deposition of Cr on α-Al_2O_3(0001) at 300 K in UHV. Analysis is done at grazing incidence (60° off normal) on the vacuum annealed alumina surface (red dots and red line) and after deposition of 0.8 Å of Cr (blue line): a) O 1s core level; b) Al 2s core level.

2. Computational results

As to get an unbiased insight into local structural and electronic characteristics of Cr adsorbates at the alumina surface under different hydroxylation conditions, surface configurations in which a single Cr adatom coexists with a hydroxylation layer composed of *n* oxygen and *m* hydrogen atoms (n, m = 0 to 3) in the (1x1) surface unit cell were systematically scrutinized by DFT approach. Table 2 summarizes the adatom electronic [Bader charges Q_{Cr} (e) and magnetic moments μ_{Cr} (μ_B)] and structural [Cr-O bonds lengths(Å)] characteristics relevant for a comparison with the present experiments. Moreover, Table 2 reports also similar results for a few configurations in which the Cr adatom substitutes the terminal surface Al cation, e.g., as a result of Cr adsorption at a surface Al vacancy. Key configurations are plotted in Fig. 4.

Configuration	Composition of the hydroxylation layer	Electronic characteristics of the Cr adatom			Structural characteristics of the Cr adatom		Average Cr-O distance (Å)
	On Hm	Q_{Cr}	μ_{Cr}	Cr^{Z+}	With Al_2O_3 substrate	With OH layer	
Cr adatom							
Cr	0 0	+0.8	4.1	0	2.15, 2.15, 2.15		2.15
Cr+H	0 1	+0.8	4.6	1	2.21, 2,24, 2.26		2.24
Cr+O	1 0	+1.3	3.8	2	2.03, 2.29, 2.39;	1.88	2.15
$Cr+H_2$	0 2	+1.1	3.7	2	2.05, 2.09, 2.13		2.09
$Cr+OH_2$	1 2	+1.2	3.7	2	2.05, 2.08, 2.16;	2.00	2.07
Cr+OH	1 1	+1.5	2.8	3	1.94, 2.12, 2.19;	1.77	2.01
$Cr+OH_3$	1 3	+1.5	2.8	3	1.99, 2.04, 2.04;	1.93	2.00
$Cr+O_2H$	2 1	+1.6	2.7	3	1.96, 2.02, 2.17	1.76, 1.88	1.96
$Cr+O_3H_3$	3 3	+1.7	2.7	3	1.98, 1.98, 1.99;	1.92, 1.92, 1.92	1.95
$Cr+H_3$	0 3	+1.7	2.7	3	2.02, 2.02, 2.03		2.02
$Cr+O_2H_2$	2 2	+1.7	2.0	4	1.99, 2.01, 2.10;	1.71, 1.89	1.94
$Cr+O_2$	2 0	+1.7	1.9	4	1.93, 2.16, 2.18;	1.69, 1.69	1.93
$Cr+O_3H_2$	3 2	+1.9	1.9	4	1.99, 2.00, 2.09;	1.70, 1.87, 1.93	1.93
$Cr+O_3H$	3 1	+2.0	1.0	5	2.02, 2.11, 2.12;	1.65, 1.68, 1.87	1.91
$Cr+O_2H_3$	2 3	+1.6	0.9	5	2.07, 2.09, 2.14;	1.72, 1.84	1.97
$Cr+O_4H$	4 1	+2.0	0.1	6	2.10, 2.13, 2.14;	1.65, 1.66, 1.67	1.89
$Cr+O_3$	3 0	+2.0	0.0	6	2.12, 2.13, 2.13;	1.65, 1.65, 1.65	1.89
$Cr+O_4$	4 0	+2.0	0.0	6	2.16, 2.17, 2.20;	1.65, 1.70, 1.73, 1.99	1.94
Cr substitution							
$-Al+Cr+H_3$	0 3	+0.4	4.9	0/1	2.30, 2.31, 2.31		2.31
-Al+Cr	0 0	+1.6	2.8	3	1.79, 1.79, 1.80		1.79
$-Al+Cr+OH_2$	1 2	+1.6	2.8	3	1.82, 1.82, 2.15	1.80	1.90
-Al+Cr+OH	1 1	+1.9	1.8	4	1.79, 1.79, 1.80	1.78	1.79

Table 2. Calculated electronic and structural characteristics of Cr ad-atoms and surface Cr substitutions obtained for different compositions of the hydroxylation layer O_nH_m: Bader charges Q_{Cr} (e), magnetic moments μ_{Cr} (μ_B), oxidation states Cr^{z+}, Cr-O bond lengths (Å) between Cr and O atoms in both the alumina substrate and the hydroxylation layer. The results are ordered by the decreasing values of Cr magnetic moment μ_{Cr}.

At the bare alumina surface, a quasi-isolated Cr adatom [a single Cr adatom per (2x2) unit cell] adsorbs preferentially in the hollow site in the direct prolongation of the corundum lattice (site labelled Al_3 in Fig. 1) with adsorption energy E_{ads} = 1.67 eV/Cr (Q_{Cr} = +0.6 e, μ_{Cr} = 4.9 μ_B), and forms three 2.15 Å long Cr-O bonds. Despite their non-vanishing Bader charges Q_{Cr}, the isolated Cr adatoms do not reduce the alumina surface, in agreement with photoemission experiments (Fig. 3a). These adsorption characteristics are similar to those reported in Table 2 (configuration labelled Cr, obtained for a single Cr adatom per (1x1) unit cell), with the same preferential adsorption site, but a somewhat larger adsorption energy E_{ads} = 2.15 eV/Cr. As a reference, in the calculated bulk corundum Cr_2O_3

structure each Cr cation (Q_{Cr} = +1.6 e, μ_{Cr} = 2.8 μ_B) forms three shorter (1.96 Å) and three longer (2.03 Å) Cr-O bonds, the average of which coincides perfectly with the experimental value (Table 1).

Regarding the calculated charge state of Cr, if the computed Bader charges do not directly represent the formal charge of the adatoms, a joint analysis of Q_{Cr} and μ_{Cr} provides a fairly good insight into the Cr oxidation state. In particular, configurations with Q_{Cr} ~ +1.2 e and μ_{Cr} ~ 3.8 μ_B clearly represent the +2 oxidation state (compared to Q_{Cr} = +1.3 e and μ_{Cr} = 3.8 μ_B calculated for bulk CrO), configurations where Q_{Cr} ~ +1.6 e and μ_{Cr} ~ 2.7 μ_B represent the +3 oxidation state (compared to Q_{Cr} = +1.6 e and μ_{Cr} = 2.8 μ_B obtained for bulk Cr_2O_3), and configurations with Q_{Cr} ~ +1.7 e and μ_{Cr} ~ 1.9 μ_B represent the +4 oxidation state (compared to Q_{Cr} = +1.7 e and μ_{Cr} = 1.9 μ_B in calculated bulk CrO_2). Similarly, configurations with Q_{Cr} ~ +1.8 e / μ_{Cr} ~ 1.0 μ_B and Q_{Cr} ~ +2.0 e / μ_{Cr} ~ 0.0 μ_B can be associated with Cr oxidation states +5 and +6, respectively. Our results show that the Cr electronic characteristics cannot be deduced solely from the composition of the hydroxylation layer. Indeed, while oxygen atoms systematically adopt their O^{-2} state, the charge state of hydrogen atoms varies between +1 and -1 depending on their local environment.

Also the average Cr-O distances $d_{Cr\text{-}O}$ do not provide a fully unambiguous indicator of the Cr oxidation state *z*. Indeed, if the average $d_{Cr\text{-}O} > 2.05$ Å for $z \leq +2$, 1.92 Å $\leq d_{Cr\text{-}O} < 2.02$ Å for $z = +3$ and +4, and $d_{Cr\text{-}O} < 1.91$ Å for $z = +5$ and +6, there exist configurations which do not follow this pattern (e.g., $Cr{+}O_2H_3$ and $Cr{+}O_4$, and those with Cr substitution). This shows that, while a progressive reduction of $d_{Cr\text{-}O}$ as a function of the Cr oxidation state *x* is indeed expected from the reduction of the Cr ionic radii (e.g., Shannon effective ionic radii), the interplay between the different character and ratio of Cr-O bonds formed with oxygen atoms of the hydroxylation layer and with those of the alumina substrate (Table 2) impacts non-negligibly the behavior of the average $d_{Cr\text{-}O}$.

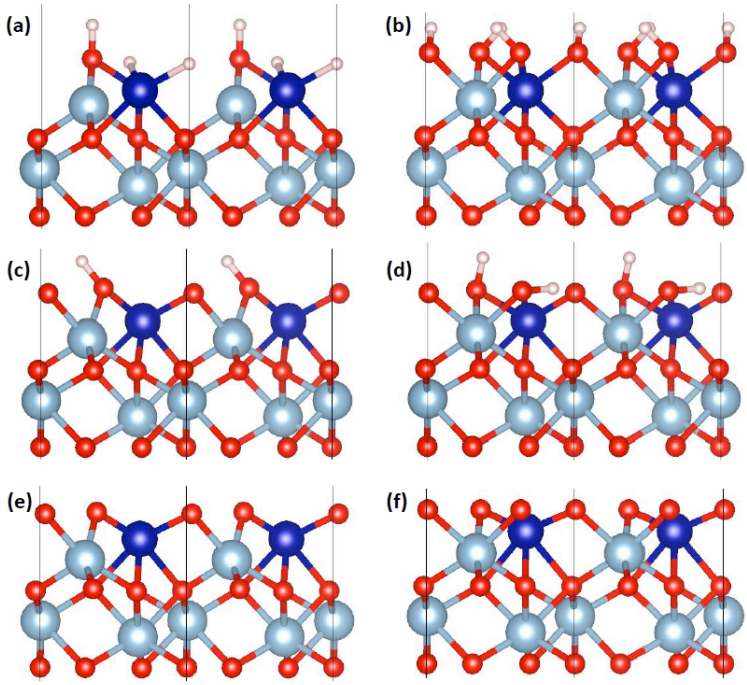

Fig 4. Atomic structures of the six thermodynamically stable surface configurations: $Cr{+}OH_3$ (a), $Cr{+}O_3H_3$ (b), $Cr{+}O_2H$ (c), $Cr{+}O_3H_2$ (d), $Cr{+}O_2$ (e), and $Cr{+}O_3$ (f). Oxygen, aluminum, chromium, and hydrogen atoms are represented by red, light blue, dark blue and small white spheres, respectively.

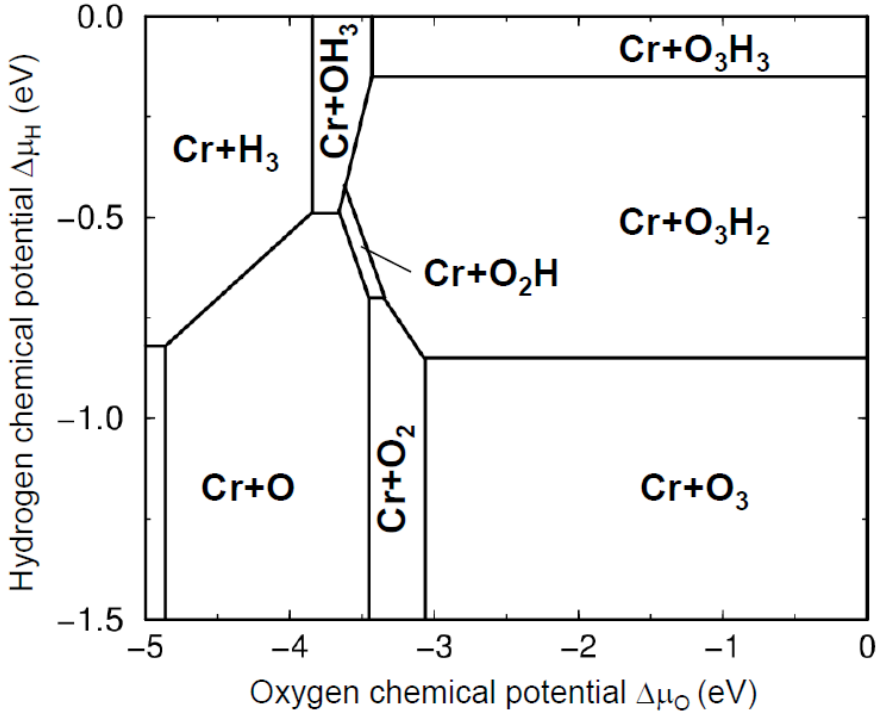

Fig 5. Calculated thermodynamic stability diagram of alternative $Cr+O_nH_m$ configurations of Cr ad-atom with hydroxylation layers of different compositions listed in Table 2, as a function of oxygen and hydrogen chemical potentials.

As to identify the most relevant structural arrangements, we have further evaluated the relative stability of ad-atom configurations from Table 2, as a function of oxygen and hydrogen chemical potentials (Fig. 5). We found that essentially six configurations may be thermodynamically stable under experimental oxygen conditions (the most oxygen-poor conditions, p_{O2} ~10^{-6} mbar at 1500 K corresponds to $\Delta\mu_O$ ~ -3.0 eV): $Cr+OH_3$, $Cr+O_3H_3$, $Cr+O_2H$, $Cr+O_3H_2$, $Cr+O_2$ and $Cr+O_3$. Their atomic structures are represented in Fig. 4. The six configurations display a significantly different character, with formal Cr oxidation states ranging from +3 (Fig. 4a-c), through +4 (Fig. 4d-e), up to +6 (Fig. 4f). In the $Cr+OH_3$ configuration, the Cr^{3+} charge state is due to a single OH^- group and two Cr-bonded H^- ions, while in the $Cr+O_2H$ one, the two H^- are replaced by a single two-fold coordinated O^{2-} anion. The $Cr+O_3H_3$ configuration is obtained by adsorption of a single neutral H_2O molecule to this latter structure. Alternatively, an additional OH^- group induces a higher Cr^{4+} oxidation state in the $Cr+O_3H_2$ configuration. The $Cr+O_2$ configuration is obtained from the $Cr+O_3H_2$ one by desorption of a single neutral H_2O molecule per surface unit cell. Finally, the three O^{2-} anions are responsible for the highest 6+ cation state in the $Cr+O_3$ configuration. We note that, aside the hydrogen-rich $Cr+OH_3$, and the hydrogen-poor $Cr+O_3$ structures, which are characterized by relatively long and short average Cr-O bond lengths (2.00 Å and 1.89 Å, respectively), the four remaining thermodynamically stable configurations are characterized by average Cr-O distances of 1.93 Å ≤ d_{Cr-O} ≤ 1.96 Å, consistent with the experimental indication (Table 1).

3. Discussion

To bridge the experimental results and the calculated adsorbate structures, we have systematically checked the matching between the principal experimental signatures and the electronic and structural

characteristics of the predicted surface configurations (Table 2). Based on the experimental results, three criteria were retained, including an oxidation state z of 3+ or 4+ and more than three oxygen nearest neighbors for the Cr atoms as well as an average Cr-O distance $d_{Cr\text{-}O}$ of about 1.95 Å (Table 1). As schematized in Fig. 6, these three concomitant criteria directly eliminate the computed configurations with $z \leq 2$. In particular, Cr adatoms at the bare alumina surface, with Cr-O bond lengths of 2.15 Å, are clearly at odds with the experimental findings and can be definitely discarded. For the same reasons, the configurations with $z \geq 5$ can also be safely discarded. We note that the surface configurations issued from Cr adsorption at surface aluminum vacancies (labelled Cr substitutions in Table 2) are systematically characterized by average Cr-O distances which are too short to fit the experimental findings.

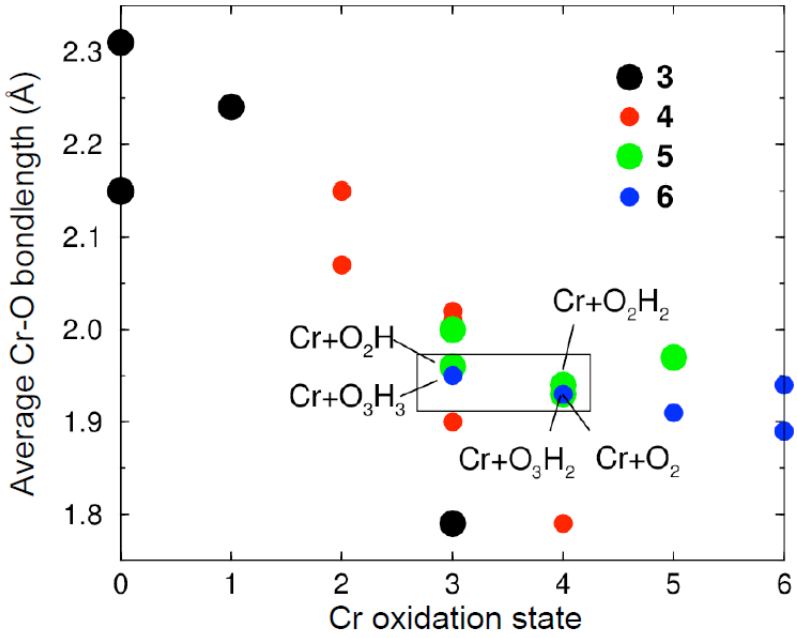

Fig 6. Calculated average Cr-O bond lengths for the configurations in Table 2 plotted as a function of Cr oxidation state. Additionally, the total number of Cr-O bonds (per Cr ad-atom) is indicated in black (3), red (4), green (5), or blue (6). Configurations with characteristics which closely approach the experimental results are highlighted.

Among the six thermodynamically stable configurations (Fig. 4), the $Cr{+}O_3H_3$, $Cr{+}O_2H$, $Cr{+}O_3H_2$, and $Cr{+}O_2$ ones match closely the main experimental evidences (Fig. 6). Moreover, the thermodynamically less stable $Cr{+}O_2H_2$ configuration also fulfills charge and distance constraints (Fig. 6). The structural models were then compared to the experimental EXAFS data. The distances and coordination numbers determined by DFT are set fixed in an Artemis fitting procedure. The coordination numbers introduced in the analysis are accounting for the polarization effect. Indeed, the light is linearly polarized along the x axis and the apparent coordination reads 3 $\cos^2(\Theta)$ for each neighbor, where Θ is the angle between the photon electric field and the interatomic vector. Therefore, the Debye-Waller factors are the only free parameters for the Cr-O pairs. The phase functions of these Cr-O pairs are extracted from the above mentioned FEFF9 calculation applied and checked on chromium oxide while those of the Cr-Al pairs come from the same procedure applied to a Cr_5Al_8 compound. Because the overall electronic configuration of Cr_5Al_8 should be different from that of Cr in our samples, these contributions from Al atoms are left free in the fitting.

5.1 The Cr+O_2H and Cr+OH configurations

We find that the Cr+O_2H configuration is the only one that displays a satisfactory agreement with the experiment (Fig. 7). In the other cases, the fitting procedure either returns non-physical values for some Debye-Waller factors, or ignores the Al contribution (left free) or even is unable to find any correct agreement. The simulated EXAFS of the computed Cr+O_2H configuration (Fig. 4c) is compared in Fig. 7 to the experiment in the case of the very low Cr coverage (0.24 Å, Table 1) in which Cr^{3+} ions are isolated on the surface as shown by the absence of a Cr-Cr bond signature in EXAFS. The model (Fig. 4c) corresponds to a 5-fold coordinated Cr^{3+} ion on a hydroxylated alumina surface. It is surrounded by three oxygens from the alumina substrate at 1.96, 2.02 and 2.17 Å, two extra oxygen atoms at 1.76 and 1.88 Å, while 2.5 Al atoms are found at 2.43 Å (these two last parameters being left free in the fitting procedure). The only weak point of the Cr^{3+}-O_2H model (Fig. 4c) is the short (2.43 Å) Cr-Al distance returned by the EXAFS fit (Fig. 7), as compared to the 2.8 Å given by DFT.

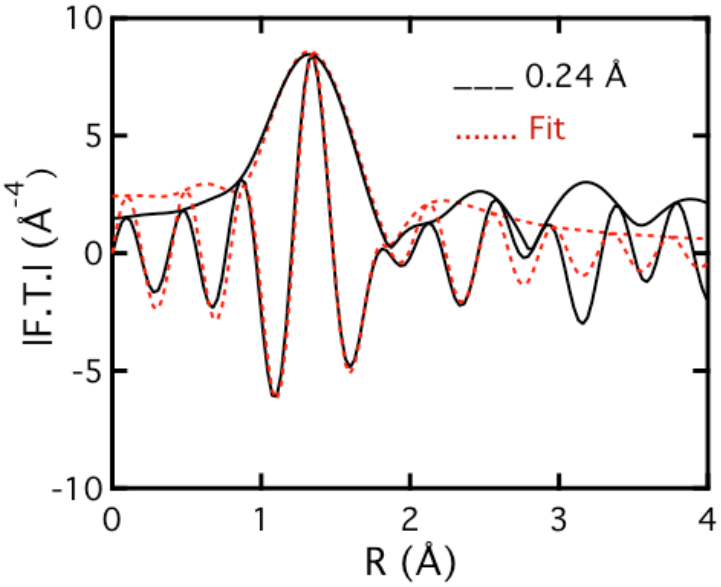

*Fig. 7– Comparison between the magnitude and imaginary parts of the Fourier transform (F.T.) for a 0.24 Å thick Cr/α-Al_2O_3(0001) film (black lines) and the theoretical result (red lines) based on the structural model presented in Fig. 4b (*Cr+O_2H site*, see text).*

The Cr+OH configuration (Table 2) deserves some comment. It corresponds to the idea of a largely dehydroxylated surface on which isolated OH groups can be found. In the presence of a unique OH group adsorbed at the alumina surface, DFT calculations show that Cr adatoms form 4-fold coordinated Cr^{3+} ions. Such a Cr charge state is enabled by the dissociation of the OH group and the negative charge of the hydrogen atom. The configuration could solve the apparent contradiction between the high oxidation state of Cr and the poor OH coverage of the alumina surface. The Ti/α-Al_2O_3(0001) raises a similar question. The amount of Ti^{4+} ions formed upon deposition of Ti on α-Al_2O_3(0001) seems to exceed what can be expected from the OH coverage available[25]. The same EXAFS analysis which was conducted on the Cr+O_2H configuration has also been done on Cr+OH. A

good agreement can be obtained, but at the expense of a very large Debye-Waller factor for two Cr-O distances. An additional argument comes from a calculation of the near edge structure of the two configurations done with the use of the *ab initio* Finite-Difference Method Near-Edge Spectra (FDMNES) to solve the Schrödinger equation. Fig 8 shows that these calculations agree definitely better with the Cr + O_2H configuration than with Cr+OH, thus confirming both the EXAFS analysis.

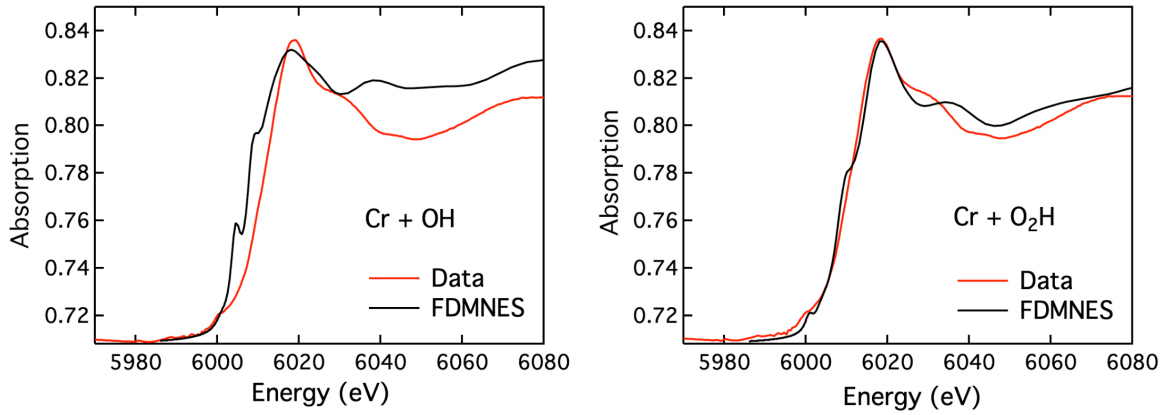

Fig. 8– Calculations of the Cr K near edge structure done by using the ab initio *Finite-Difference Method Near-Edge Spectra (FDMNES) for a 1.05 Å thick Cr/α-Al_2O_3(0001) film: left: Cr+OH - right: Cr+O_2H.*

5.2. Stability at different O_nH_m coverage

The above comparison and discussion show that the electronic and atomic structures of the Cr+O_2H configuration match particularly well the corresponding experimental signatures. However, we note that this configuration appears only quite marginally in the computed stability diagram (Fig. 5). Indeed, it is stable in a particularly narrow range of oxygen and hydrogen chemical potentials and its formation energy is only a little lower than those of the neighboring configurations**.**

However, the experimental situation may not correspond to the global thermodynamic equilibrium. Indeed, if the alumina surface on which Cr is deposited is likely partially covered by surface hydroxyl groups, their density and the precise composition of this hydroxylation layer are essentially unknown. Upon adsorption of a small quantity of Cr adatoms the hydroxylation layer restructures as to create locally the most thermodynamically favored Cr+O_nH_m surface complexes. Such restructuration may be limited by two factors. On the one hand, in the presence of a small fraction of the hydroxylation layer, the existing surface hydroxyls may be insufficient for the formation of the most favored Cr+O_nH_m complexes. On the other hand, their formation may be hindered by the kinetics of surface diffusion. As a consequence, Cr adsorbates may find themselves in a less oxygen-rich environment than required for their thermodynamic stability. Such a key role of kinetics in surface ordering is reminiscent of the order of formation of new facets during the dissolution of cubic MgO smoke particles initially exhibiting (100) orientations. Although the morphology of the crystallites that are derived from surface energies computed within the density functional theory (DFT) only involve (100) and (111) facets, (110) facets appear first. The unexpected presence of (110) cuts was explained via a ‘‘constrained’’ Wulff equilibrium shape that arises from slower kinetics for the formation of (111) facets with respect to (110)[63].

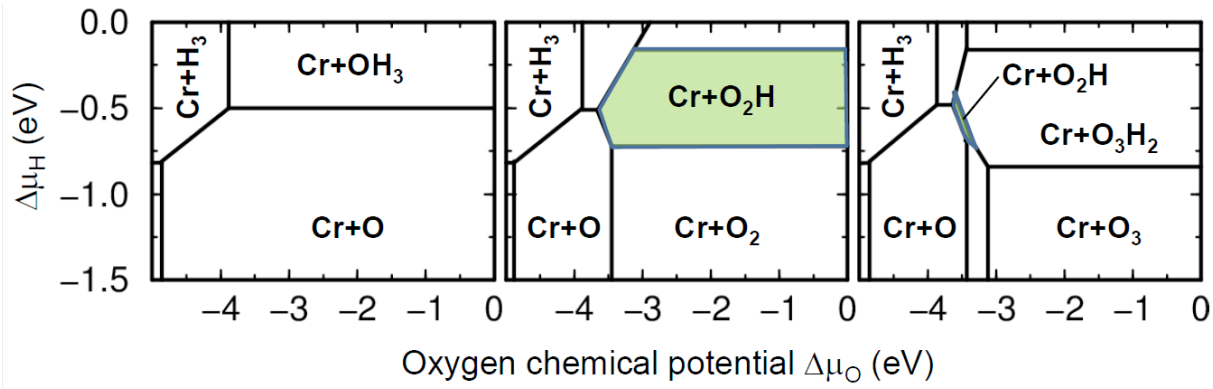

Fig. 9 - Calculated stability diagrams of surface configurations involving a Cr ad-atom and hydroxylation layers of different compositions from Table 2, as a function of oxygen and hydrogen chemical potentials. The three diagrams have been obtained under an additional constrain on the maximal number of oxygen atoms (per surface unit cell) n_{max} = 1, 2, and 3 (left to right). Note that the diagram obtained for n =3 corresponds to that in Fig. 5. The Cr+O_2H configuration which matches the best the experimental signatures is shown in green.

As to mimic the effect of the limited availability of adsorbed oxygen for the oxidation reaction of Cr, we have recalculated the stability diagrams with an additional constraint on the maximal number of oxygen atoms in the hydroxylation layer (per surface unit cell). Fig. 9 clearly shows that, if the oxygen-dense configurations (Cr+O_3H_m) cannot form, those with a smaller oxygen density (Cr+O_2H_m for n_{max} = 2 and Cr+O_1H_m for n_{max} = 1) become thermodynamically stable. Interestingly, the Cr+O_2H configuration, which displays the best matching with the experimental signatures, turns out to be the most stable (n_{max} = 2) in a particularly large range of oxygen and hydrogen conditions. Beyond the stability of the Cr^{3+}+O_2H moiety, a plausible assumption is the formation of (Cr,OH) patches in which OH groups are shared by Cr ions. In the absence of long-range order of the OH coverage[34], Cr deposition on alumina at low coverage likely results in a mixing of configurations involving Cr ions and surface OH groups. Indeed, DFT (See Section 5.1) demonstrates that even adsorption of Cr at the vicinity of isolated OH can produce Cr^{3+} ions, provided the proton of the hydroxyl groups behaves as an electron acceptor and forms a H-ion adsorbed on a surface cation. This configuration is clearly unstable if isolated (See Section 5.1). However, its appearance within (Cr,OH) surface complexes is not to be excluded.

5.3. Hydroxylation of the annealed α-Al_2O_3(0001) surface

The combination of EXAFS analysis and DFT calculation demonstrates unambiguously the presence of hydroxyl groups at the surface of α-Al_2O_3(0001) annealed in UHV up to a temperature which is just below the onset of reconstruction[30-33]. On α-Al_2O_3(0001), the residual hydroxyl coverage[25,33] was estimated to range between 1.8×10^{14} and 3×10^{14} OH.cm^{-2} while the amount of OH groups which can be reversibly adsorbed is reproducibly found in the $5\text{-}6\times10^{14}$ OH.cm^{-2} coverage range[13,14,24,25]. These observations are generalized by the detection of a similar residual coverage of 2.6 OH.nm^{-2} on nanocrystalline α-Al_2O_3 [6], although the diversity in surface orientations prevents a direct comparison with the α-Al_2O_3(0001) surface. The lowest Cr deposit prepared herein (0.24 Å) corresponds to ~ 2×10^{14} Cr atom.cm^{-2} which can reasonably be associated to the formation of (Cr,OH) surface complexes dominated by Cr^{3+}-O_2H configurations.

The existence of residual surface OH groups at the α-Al_2O_3(0001) is of paramount importance as regards the physico-chemical behavior of that surface. More specifically, it might explain the observed systematic discrepancies between relaxations found by surface X-ray diffraction recorded on the supposedly bare Al-terminated α-Al_2O_3(0001) and the theoretical DFT models[64-65].

6. Conclusion

Absorption spectra recorded at the Cr K edge on Cr/α-Al_2O_3(0001) thin films, supported by a density functional modeling of the Cr sites, clearly evidence an environment which requires the existence of hydroxyl groups on the alumina surface:

- The near edge structure determines the electronic configuration of chromium as Cr^{3+} and the EXAFS analysis evidences a Cr environment similar to that found in Cr_2O_3.
- Most importantly, this environment involves 4 oxygen atoms, which suggest the presence of surface OH groups since photoemission shows that Cr deposition, that does not entail a reduction of the alumina surface, results in a O 1s chemical shift.
- Indeed, none of the DFT models based on bare alumina, that return Cr-O distances much larger than experimental values, succeed in explaining the local environment of Cr found by EXAFS.
- The hint comes from a parallel between experimental data and a comprehensive DFT study of the Cr^{z+}-O_nH_m / α-Al_2O_3(0001) configurations (z=0 to 6, n and m=0 to 3). The Cr^{3+}-O_2H / α-Al_2O_3(0001) DFT model gives definitely the best agreement with the data, as demonstrated by the fitting of the experimental spectra with the Fourier transform derived from theoretical configurations and calculated near-edge spectra.

Therefore, the local environment of adsorbed Cr acts as a probe to demonstrate that the annealed α-Al_2O_3(0001)-(1×1) surface retains a partial OH coverage even after high temperature treatment. At the same time, the structural site of Cr at the initial stages of the deposition has been determined. The *a priori* disordered OH adlayer suggests the formation of (Cr,OH) surface complexes dominated by the Cr^{3+}-O_2H / α-Al_2O_3(0001) configuration.

Acknowledgements. We thank the team in charge with the SOLEIL machine and Damien Roy (LUCIA beamline) for his technical assistance. This work was supported by the French State Fund managed by the ANR within the Investissements d'Avenir program under Reference No. ANR-11-IDEX-0004-02, and more specifically within the framework of the Cluster of Excellence MATISSE.

References

(1) Wang, Y.; Michel, F. M.; Choi, Y.; Eng, P. J.; Levard, C.; Siebner, H.; Gu, B.; Bargar, J. R.; Brown, G. E. Jr. Pb, Cu, and Zn distributions at humic acid-coated metal-oxide surfaces. *Geochim. Cosmochim. Acta* **2016**, *188*, 407-423.

(2) Musorrafiti, M. J.; Konek, C. T.; Hayes, P. L.; Geiger, F. M. Interaction of Chromium(VI) with the α-Aluminum Oxide−Water Interface. *J. Phys. Chem. C* **2008**, *112*, 2032-2039.

(3) Bara, C.; Plais, L.; Larmier, K.; Devers, E.; Digne, M.; Lamic-Humblot, A. F.; Pirngruber, G. D.; Carrier, X. Aqueous-Phase Preparation of Model HDS Catalysts on Planar Alumina Substrates: Support Effect on Mo Adsorption and Sulfidation. *J. Am. Chem. Soc.* **2015**, *137*, 15915-15928.

(4) Chambers, S.; Droubay, T.; Jennison, D.; Mattsson, T. Laminar Growth of Ultrathin Metal Films on Metal Oxides: Co on Hydroxylated α-Al_2O_3(0001). *Science* **2002**, *297*, 827-831.

(5) Cao, X. Q.; Vassen, R.; Stoever, D. Ceramic materials for thermal barrier coatings. *J. European Ceram. Soc.* **2004**, *24*, 1-10.

(6) McHale, J. M.; Auroux, A.; Perrotta, A. J.; Navrotsky, A. Surface Energies and Thermodynamic Phase Stability in Nanocrystalline Aluminas. *Science* **1997**, *277*, 788-791.

(7) Abriou, D.; Jupille, J. Self-inhibition of water dissociation on magnesium oxide surfaces. *Surf. Sci. Lett*. **1999**, *430*, L527-L532.

(8) Ončák, M.; Włodarczyk, R.; Sauer, J. Water on the MgO(001) Surface: Surface Reconstruction and Ion Solvation. *J. Phys. Chem. Lett.* **2015**, *6*, 2310-2314.

(9) Coustet, V. ; Jupille, J. Hydroxyl groups on oxide surfaces. *Nuovo Cimento D* **1997**, *19*, 1657-1664.

(10) Liu, P.; Kendelewicz, T.; Brown, G. E.; Nelson, E. J.; Chambers, S. A Reaction of water vapor with *α*-Al_2O_3(0001) and *α*-Fe_2O_3(0001) surfaces: synchrotron X-ray photoemission studies and thermodynamic calculations. *Surf. Sci.* **1998**, *417*, 53-65.

(11) Chen, J. G.; Crowell, J. E.; Yates, Jr. J. T. Assignment of a surface vibrational mode by chemical means: Modification of the lattice modes of Al_2O_3 by a surface reaction with H_2O. *J. Chem. Phys.* **1986**, *84*, 5906.

(12) Coustet, V.; Jupille, J. High−resolution electron−energy−loss spectroscopy of hydroxyl groups at the surface of bulk insulating oxides. *Surf. Interface Anal.***1994**, *22*, 280-283.

(13) Coustet, V.; Jupille, J. High-resolution electron-energy-loss spectroscopy of isolated hydroxyl groups on α-Al_2O_3(0001). *Surf. Sci.* **1994**, *307-309*, 1161-1165.

(14) Elam, J. W.; Nelson, C. E.; Cameron, M. A.; Tolbert, M. A.; George, S. M. Adsorption of H_2O on a Single-Crystal α-Al_2O_3(0001) Surface. *J. Phys. Chem. B* **1998**, *102*, 7008-7015.

(15) Hass, K. C.; Schneider, W. F.; Curioni, A.; Andreoni, W. The Chemistry of Water on Alumina Surfaces: Reaction Dynamics from First Principles. *Science* **1998**, *282*, 265-268.

(16) Ranea, V. A.; Carmichael, I.; Schneider, W. M. DFT Investigation of Intermediate Steps in the Hydrolysis of α-Al_2O_3(0001). *J. Phys. Chem. C* **2009**, *113*, 2149–2158.

(17) P. Thissen, P.; Grundmeier, G.; Wippermann, S.; Schmidt, W. G. Water adsorption on the α-Al_2O_3(0001) surface. *Phys. Rev. B* **2009**, *80*, 245403.

(18) Sterrer, M.; Freund, H.-J. Towards Realistic Surface Science Models of Heterogeneous Catalysts: Influence of Support Hydroxylation and Catalyst Preparation. Method, *Catal. Lett.* **2013**, *143*, 375-385.

(19) Libuda, J.; Frank, M.; Sandell, A.; Andersson, S.; Brühwiler, P.A.; Bäumer, M.; Mårtensson N.; Freund, H.-J. Interaction of rhodium with hydroxylated alumina model substrates. *Surf. Sci.* **1997**, *384*, 106-119.

(20) Heemeier, M.; Frank, M.; Libuda, J.; Wolter, K.; Kuhlenbeck, H.; Bäumer, M.; Freund, H. J. The influence of OH groups on the growth of rhodium on alumina: a model study. *Catal. Lett.* **2000**, *68*, 19-24.

(21) Cavallotti, R.; Le, H. L. T.; Goniakowski, J.; Lazzari, R.; Jupille, J.; Koltsov, A.; Loison, D. New routes for improving adhesion at the metal/α-Al_2O_3(0001) interface. *Phys. Chem. Chem. Phys.* **2016**, *18*, 3032-3039.

(22) Shi, X.-R; Sholl, D. S. Nucleation of Rh_n (n = 1−5) Clusters on γ-Al_2O_3 Surfaces: A Density Functional Theory Study. *J. Phys. Chem. C* **2012**, *116*, 10623−10631.

(23) Ravenelle, R. M.; Copeland, J. R.; Kim, W.-G.; Crittenden, J. C.; Sievers, C. Structural changes of γ-Al_2O_3-supported catalysts in hot liquid water. *ACS Catal.* **2011**, *1*, 552−561.

(24) Lazzari, R.; Jupille, J. Chemical reaction via hydroxyl groups at the titanium/α-Al_2O_3(0001) interface. *Surf. Sci.* **2002,** *507–510*, 683-687.

(25) Lazzari, R.; Jupille, J. Wetting and interfacial chemistry of metallic films on the hydroxylated α−Al_2O_3(0001) surface. *Phys. Rev. B* **2005***, 71*, 045409.

(26) Cavallotti, R.; Le, H. L. T.; Goniakowski, J.; Lazzari, R.; Jupille, J.; Koltsov, A.; Loison, D. Role of Surface Hydroxyl Groups on Zinc Adsorption Characteristics on α-Al_2O_3(0001) Surfaces: First-Principles Study. *J. Phys. Chem. C* **2014**, *118*, 13578−13589.

(27) Le, H. L. T.; Lazzari, R.; Goniakowski, J.; Cavallotti, R.; Chenot, S.; Noguera, C.; Jupille, J.; Koltsov, A.; Mataigne, J. M. Tuning Adhesion at Metal/Oxide Interfaces by Surface Hydroxylation. *J. Phys. Chem. C* **2017**, *121*, 11464-11471.

(28) Niu, C.; Shepherd, K.; Martini, D.; Tong, J.; Kelber, J.; Jennison, D.; Bogicevic, A. Cu interactions with α-Al_2O_3(0001): effects of surface hydroxyl groups versus dehydroxylation by Ar-ion sputtering. *Surf. Sci.* **2000**, *465*, 163-176.

(29) Kelber, J.A.; Niu, C.; Shepherd, K.; Jennison, D.R.; Bogicevic, A. Copper wetting of α-Al_2O_3(0001): theory and experiment. *Surf. Sci.* **2000**, *446*, 76-88.

(30) French, T. M.; Somorjai, G. A. Composition and surface structure of the (0001) face of α-alumina by low-energy electron diffraction. *J. Phys. Chem.* **1970,** *74*, 2489-2495.

(31) Gautier, M.; Duraud, J. P.; Van, L. P.; Guittet, M. J. Modifications of α-Al_2O_3(0001) surfaces induced by thermal treatments or ion bombardment. *Surf. Sci*. **1991**, *250*, 71-80.

(32) Renaud, G.; Villette, B. and Vilfan, I. and Bourret, A., Atomic structure of the α-Al_2O_3(0001)-(√31x√31)R±9°. *Phys. Rev. Lett*., **1994**, *73*, 1825-1828.

(33) Renaud, G. Oxide surfaces and metal/oxide interfaces studied by grazing incidence X-ray scattering. *Surf. Sci. Rep.* **1998**, *32*, 5-90.

(34) Ahn, J.; Rabalais, J W. Composition and structure of the Al_2O_3{0001}-(1 × 1) surface. *Surf. Sci.* **1997**, *388*, 121-131.

(35) Fu, Q.; Wagner, T.; Rühle, M. Hydroxylated α-Al_2O_3 (0001) surfaces and metal/α-Al_2O_3 (0001) interfaces. *Surf. Sci.* **2006***, 600*, 4870-4877.

(36) Kirsch, H.; Wirth, J.; Tong, Y.; Wolf, M.; Saalfrank, P.; Campen, R. K. Experimental Characterization of Unimolecular Water Dissociative Adsorption on α-Alumina. *J. Phys. Chem. C* **2014**, *118*, 13623−13630.

(37) Tong, Y.; Wirth, J.; Kirsch, H.; Wolf, M.; Saalfrank, P.; Campen, R. K. Optically probing Al—O and O—H vibrations to characterize water adsorption and surface reconstruction on α-alumina: An experimental and theoretical study. J. Chem. Phys. **2015**, *142*, 054704.

(38) Petrik, N. G.; Huestis, P. L.; LaVerne, J. A.; Aleksandrov, A. B.; Orlando, T. M.; Kimmel G. A. Molecular Water Adsorption and Reactions on α-Al_2O_3(0001) and α-Alumina Particles. *J. Phys. Chem. C* **2018**, *122*, 9540-9551.

(39) Chopra, K. L.; Paulson, P. D.; Dutta, V. Thin-film solar cells: An overview. *Progress in Photovoltaics* **2004**, *12*, 69-92.

(40) Sondergard, E.; Kerjan, O.; Barreteau, C.; Jupille, J. Structure and growth of titanium buffer layers on Al_2O_3(0001). *Surf. Sci.* **2004**, *559*, 131-140.

(41) Brandenburg, J.; Huhne, R.; Schultz, L.; Neu, V. Domain structure of epitaxial Co films with perpendicular anisotropy. *Phys. Rev. B* **2009**, *79*, 054429.

(42) Le, H. L. T ; Goniakowski. J.; Noguera, C.; Koltsov, A.; Mataigne. J. M. Improving Adhesion at the Alumina/Zinc Interface by Stainless Steel Buffers. *J. Phys. Chem. C* **2017**, *121*, 25143−25151.

(43) Le, H. L. T.; Goniakowski, J.; Noguera, C.; Koltsov, A.; Mataigne, J. M. First-Principles Study on the Effect of Pure and Oxidized Transition- Metal Buffers on Adhesion at the Alumina/Zinc Interface. *J. Phys. Chem. C* **2016**, *120***,** 9836−9844.

(44) Flank, A.-M.; Delaunay, R.; Lagarde, P.; Pompa, M.; Jupille, J. Epitaxial silver layer at the MgO(100) surface. *Phys. Rev. B* **1996**, *53*, R1737-1739.

(45) Lagarde, P.; Flank, A.-M.; Prado, R.; Bourgeois, S.; Jupille, J. The defined adsorption site of sodium on TiO_2(110)-(1x1). *Surf. Sci.* **2004**, *553*, 115-125.

(46) Cabailh, G.; Goniakowski, J.; Noguera, C.; Jupille, J.; Lazzari, R.; Li, J.; Lagarde, P.; Trcera, N. Evidence of a nanosize regime in oxide/metal heteroepitaxy. *Phys. Rev. Mat.* **2019**, *3*, 046001.

(47) Lazzari, R.; Goniakowski, J.; Cabailh, G.; Cavalotti, R.; Trcera, N.; Lagarde, P.; Jupille, J. Surface and epitaxial stresses on supported metal clusters. *Nano Letters* **2016**, *16*, 2574-2579.

(48) Kresse, G.; Hafner, J. *Ab initio* Molecular Dynamics for Liquid Metals. *Phys. Rev. B* **1993**, *47*, 558−561.

(49) Kresse, G.; Furthmuller, J. Efficient iterative schemes for ab initio total energy calculations using a plane-wave basis set. *Phys. Rev. B* **1996**, *54*, 11169–11186.

(50) Blöchl, P. E. Projector augmented-wave method. *Phys. Rev. B* **1994**, *50*, 17953–17979.

(51) Kresse, G.; Joubert, D. From ultra-soft pseudopotentials to the projector augmented-wave method. *Phys. Rev. B* **1999**, *59*, 1758–1775.

(52) Dion, M.; Rydberg, H.; Schroder, E.; Langreth, D. C.; Lundqvist, B. I. Van der Waals density functional for general geometries. *Phys. Rev. Lett.* **2004**, *92*, 246401.

(53) Klimes, J.; Bowler, D. R.; Michaelides, A. Chemical accuracy for the van der Waals density functional. *J. Phys.: Cond. Matt.* **2010**, *22*, 022201.

(54) Klimes, J.; Bowler, D. R.; Michaelides, A. Van der Waals Density functionals applied to solids. *Phys. Rev. B* **2011**, *83*, 195131.

(55) Bader, R. F. W. A quantum theory of molecular structure and its applications. *Chem. Rev.* **1991**, *91*, 893–928.

(56) Henkelman, G.; Arnaldsson, A.; Jonsson, H. A fast and robust algorithm for Bader decomposition of charge density. *Comput. Mater. Sci*. **2006**, *36*, 354–360.

(57) Momma, K.; Izumi, F. VESTA 3 for three-dimensional visualization of crystal, volumetric and morphology data. *J. Appl. Crystallogr.* **2011**, *41*, 1272–1276.

(58) Joly, Y. X-ray absorption near-edge structure calculations beyond the muffin-tin approximation. *Phys. Rev. B* **2001**, *63*, 125120.

(59) Hedin L.; Lundqvist, B.I. Explicit local exchange-correlation potentials. *J. Phys. C* **1971***, 4*, 2064-2083.

(60) Ravel, B.; Newville, M. *ATHENA*, *ARTEMIS*, *HEPHAESTUS*: data analysis for X-ray absorption spectroscopy using *IFEFFIT*. *J. Synchrotron Rad.* **2005**, *12*, 537-541.

(61) Rehr, J. J.; Kas, J. J.; Prange, M. P.; Sorini, A. P.; Takimoto, Y.; Vila, F. *Ab initio* theory and calculations of X-ray spectra. *Comptes Rendus Physique* **2009**, *10*, 548-559.

(62) Messaykeh, M. A fundamental approach of the wetting at Zn/Al_2O_3 interface: The effect of a Cr buffer. Ph.D. Dissertation, Sorbonne Université, Paris, **2018.**

(63) Geysermans, P.; Finocchi, F.; Goniakowski, J.; Hacquart, R.; Jupille, J. Combination of (100), (110) and (111) facets in MgO crystals shapes from dry to wet environment *Phys. Chem. Chem. Phys.* **2009**, *11*, 2228-2233.

(64) Guénard, E.; Renaud, G.; Barbier, A.; Gautier-Soyer, M. Determination of the α-Al_2O_3(0001) Surface Relaxation and Termination by Measurements of Crystal Truncation Rods. *Surf. Rev. Lett.* **1998**, *5*, 321-324.

(65) Woodruff, D. P. Quantitative Structural Studies Of Corundum and Rocksalt Oxide Surfaces *Chem. Rev.* **2013**, *113*, 3863−3886.